International Journal of Aerospace and Lightweight Structures (IJALS)

UPDATING COMPUTATIONAL AEROELASTIC MODELS USING FLIGHT FLUTTER TEST DATA

S. TIMME* and K. J. BADCOCK†

School of Engineering, University of Liverpool
Liverpool, England L63 3GH, United Kingdom

Received date
Accepted date

A method is explored to identify a correction for the system matrices of a computational aeroelastic model based on information from flight test data. The correction matrices are identified using the Nissim and Gilyard method adapted in this work to exploit the predictive capabilities of numerical aeroelastic tools while correcting for missing physics and systematic modelling errors. The simplified aerodynamics in the original Nissim and Gilyard method are discarded using computational fluid dynamics to evaluate the aerodynamic influence in the fluid/structure coupled system. Results are presented for the aeroelastic Goland wing/store and multidisciplinary optimisation wing configurations.

Keywords: Aeroelasticity; Computational Fluid Dynamics; Flutter; Model Updating; System Identification.

1. Introduction

Several techniques have been discussed in the literature to use subcritical flight flutter test data to extrapolate for the flutter speed to establish the safe flight envelope. The most widely used method, possibly due to its simplicity and robustness, is the curve fit of a typical instability indicator, such as the modal damping values, and its variation with the freestream velocity. This is in essence the method which was used in the first formal flutter test conducted by Boris von Schlippe of Junkers Airplane Company in 1935 [von Schlippe, 1936] to avoid undue risk from the then standard approach of flying the aircraft at maximum speed to demonstrate its stability. The basic procedure was to excite the components of the structure at resonant frequencies, to measure and plot the response amplitude with increasing flight speed, and to judge the test continuation from the previous results. The basic elements of flight flutter testing (excitation, data acquisition and data analysis) have remained the same ever since, although the technologies used have seen remarkable improvements, most significantly with the development of digital computers for data analysis [Kehoe, 1995].

*Research Associate, Sebastian.Timme@liverpool.ac.uk
†Professor, K.J.Badcock@liverpool.ac.uk

The damping curve fit belongs to the category of direct methods, others of which, such as the flutter margin method or the envelope function, are reviewed in the papers of Dimitriadis and Cooper [2001] and Kayran [2007]. Methods of the second category (i.e. indirect methods) aim to identify the equations of motion of the whole system (including matrices to distinguish the aerodynamic coupling) to predict the stability of the aircraft with varying flight speed. A prominent example is the method of Nissim and Gilyard [1989]. With the Nissim and Gilyard method the aeroelastic equations of motion to model the system dynamics are written as a response problem allowing forced external excitation. The system is then excited with some known input signal (e.g. a chirp) and the modal response as output is analysed and fed into the dynamics' model. An overdetermined algebraic system is formed when using more excitation frequencies than having modal degrees–of–freedom and solved for the system matrices in the common least squares sense. Thus, we are dealing with an inverse problem as spectral information is used to reconstruct matrices.

The Nissim and Gilyard method made two important assumptions. First, the simplified aerodynamics assumed in the equations of motion challenge the method's applicability in the transonic flight regime where significant variation of the aerodynamic influence can be expected [Timme and Badcock, 2011]. Indeed, we are dealing with a strictly nonlinear problem and the aerodynamic coupling matrix cannot be assumed to be constant with respect to any parameter variation. This point is addressed in this paper using computational fluid dynamics (CFD) to model the aerodynamics. Secondly, the original method implicitly neglects (nonlinear) static deformation of the structure for variation in the dynamic pressure as the matrices of generalised damping and stiffness are assumed to be constant. In Bendiksen [2008] it was argued that for flexible high aspect ratio swept wings the nonlinear static deformation plays an important role in the instability mechanism and a nonlinear structural model is required. In addition, the original method outright disregards possible advances in numerical aeroelastic modelling to complement the analysis.

In previous work by Badcock and Woodgate [2010], a small nonlinear eigenvalue problem, consisting of the structural equations corrected for the fluid/structural coupling, was solved to predict the stability of the aeroelastic system. Computational fluid dynamics methods were used to compute the aerodynamic correction term, the evaluation of which significantly influences the accuracy and efficiency of the numerical scheme, particularly in the transonic flight regime with nonlinear flow features (such as shock waves and separation) where linear aerodynamics fail. Kriging interpolation together with coordinated risk–based sampling was applied for the approximation of the aerodynamic influence matrix to search parameter spaces for aeroelastic instability and to update aerodynamic models of variable fidelity [Timme and Badcock, 2011], [Timme *et al.*, 2011].

This paper aims to explore a method to allow the use of flight flutter test data to update numerical predictions. Different to the original Nissim and Gilyard method, knowledge of the system is assumed via a numerical model which is updated based on identified corrections. Thus, rather than modelling the complete system with constant matrices, the matrices for updating are constant instead to correct a potentially nonlinear trend provided by the numerical model. The aerodynamics are evaluated by CFD simulations avoiding the shortcomings of simplified linear modelling. As realistic flight flutter test data are not available to the authors in this paper, these flight data are emulated by unsteady CFD simulations as well.

The paper continues with the presentation of the flow and structural models and the discussion of the eigenvalue stability analysis using CFD methods. Then, the original and the adapted Nissim and Gilyard methods are described together with results for the Goland wing/store configuration and the multidisciplinary optimisation (MDO) wing.

2. Models

2.1. *Flow Model*

The Euler equations are considered as the aerodynamic model in this investigation. In compact dimensionless notation, these equations, establishing a system of five coupled first order partial differential equations to describe conservation of mass, momentum and energy while neglecting viscous and heat–conduction effects, are written as

$$\frac{d}{dt}\int\limits_{\Omega(t)} \boldsymbol{w}_f \, dV + \int\limits_{\partial\Omega(t)} F \cdot \boldsymbol{n} \, dS = 0, \tag{1}$$

where the vector of fluid unknowns $\boldsymbol{w}_f$ contains density, velocity components and total energy, and F denotes the convective fluxes evaluated at the surface $\partial\Omega$ of the time–dependent control volume Ω. The governing equations are solved using a block–structured, cell–centred, finite–volume scheme for spatial discretisation [Badcock *et al.*, 2000]. The computational domain is discretised using a finite number of non–overlapping control volumes with the governing equations applied to each in turn. Convective fluxes are evaluated by the approximate Riemann solver of Osher and Chakravarthy [1983] with the MUSCL scheme [van Leer, 1979] achieving essentially second order accuracy and van Albada's limiter preventing spurious oscillations around steep gradients. Boundary conditions are enforced using two layers of halo cells.

Spatial discretisation leads to a system of n_f first order ordinary differential equations in time written in semidiscrete notation as $\dot{\boldsymbol{w}}_f = \boldsymbol{R}_f(\boldsymbol{w}_f, \boldsymbol{\eta})$ where $\boldsymbol{w}_f$ and $\boldsymbol{\eta}$ denote vectors of fluid and structural unknowns, respectively, and $\boldsymbol{R}_f$ is the fluid residual vector. The dimension of the fluid system is five times the number of control volumes. The structure influences the fluid response due to the moving fluid mesh and boundary conditions in unsteady simulations. Implicit time marching in pseudo time converges to steady state solutions, while a second order dual time stepping is used for unsteady simulations [Jameson, 1991]. Resulting linear systems are solved by a Krylov subspace iterative method applying block–incomplete lower–upper factorisation for preconditioning [Badcock and Woodgate, 2010].

2.2. *Modal Structural Model*

The structural equations of motion, a set of second order ordinary differential equations in time, are defined in physical coordinates as

$$M\delta\ddot{\boldsymbol{x}}_s + C\delta\dot{\boldsymbol{x}}_s + K\delta\boldsymbol{x}_s = q\boldsymbol{f} \tag{2}$$

where M, C and K denote matrices of mass, damping and stiffness, respectively. Commonly, the aircraft structure is represented as a linear combination of normal modes, small in number when compared with the large dimension of the CFD fluid system. The deflections $\delta\boldsymbol{x}_s$ of the (linear) structure are defined at the physical coordinates $\boldsymbol{x}_s$ by $\delta\boldsymbol{x}_s = \Phi\,\boldsymbol{\eta}$, where the vector $\boldsymbol{\eta}$ contains the n_η generalised coordinates (modal amplitudes). The columns of the matrix Φ (having dimensions $n_s \times n_\eta$) contain the mode shape vectors evaluated from a finite–element model of the structure. The structural equations in Eq. (2) are routinely transformed into the modal system and an appropriate scaling is applied to obtain generalised masses of magnitude one (i.e. $\Phi^T M \Phi = I$). This gives a system of n_η second order ordinary differential equations in time for the modal structural model written as

$$I\ddot{\boldsymbol{\eta}} + \Psi\,\dot{\boldsymbol{\eta}} + \Omega\,\boldsymbol{\eta} = q\Phi^T\boldsymbol{f}. \tag{3}$$

The generalised stiffness matrix $\Omega = \Phi^T K \Phi$ contains the n_η normal mode circular frequencies squared on the diagonal. The generalised damping matrix $\Psi = \Phi^T C \Phi$ contains the n_η values of modal damping on the diagonal with an individual term evaluated as $2\zeta\omega_\eta$ where ω_η is a normal mode circular frequency and ζ is a modal damping ratio. The vector $\boldsymbol{f}$ of aerodynamic pressure forces at the structural grid points follows from the wall pressure coefficient, the area of the surface segment and the unit normal vector, and thus is a function of fluid and structural unknowns. It is then projected using the mode shapes to obtain the n_η generalised forces $\Phi^T\boldsymbol{f}$. The mapping between the fluid and structural meshes uses the constant volume tetrahedron transformation [Goura, 2001] although other methods can be used. The dynamic pressure is denoted by q.

3. Eigenvalue Stability Formulation

For the linear stability analysis of the aeroelastic system, the development and interaction of the aeroelastic modes originating in the wind–off (uncoupled) structural system is the main concern. The linear stability analysis assumes small amplitude structural motion and a linear relationship between a structural deflection and the fluid response. Then, the system of equations in Eq. (3) is written as an eigenvalue problem for the eigenvalues $\lambda = \sigma \pm i\omega$,

$$\left\{\lambda^2\, I + \lambda\Psi + \Omega - qQ(\lambda)\right\}\hat{\boldsymbol{\eta}} = 0 \tag{4}$$

where $\boldsymbol{\eta} = \hat{\boldsymbol{\eta}}\, e^{\lambda t}$ and $\Phi^T \boldsymbol{f} = Q\, \boldsymbol{\eta}$ with Q as the aerodynamic influence matrix. A stable system has all of its eigenvalues with a negative real part, while a purely imaginary eigenvalue gives the onset of an instability of the Hopf type (i.e. flutter). The evaluation of the aerodynamic influence often significantly contributes to the overall cost of the analysis. Conventional methods applied in industrial problems use a linear aerodynamic theory, such as the doublet lattice method, corrected for its well known limitations in the transonic regime using experimental data or higher fidelity (nonlinear) flow predictions [Palacios *et al.*, 2001]. In recent years the use of high fidelity computational fluid dynamics to model the unsteady aerodynamics, particularly in the transonic regime, has become feasible, and thus an active area of investigation.

One approach, referred to as the Schur complement eigenvalue method, has first been discussed by Badcock and Woodgate [2010]. The coupled aeroelastic system of fluid and structural equations is written as a first order ordinary differential equation in time[a] and linearised about the steady state (equilibrium) solution $\boldsymbol{w}_0$,

$$\delta \dot{\boldsymbol{w}} = \boldsymbol{R}(\boldsymbol{w}_0, \mu) + A(\boldsymbol{w}_0, \mu)\, \delta \boldsymbol{w} \tag{5}$$

where $\delta \boldsymbol{w} = \boldsymbol{w} - \boldsymbol{w}_0$ is the joined vector of unknowns of the fluid and structural systems and $\boldsymbol{R}$ contains the corresponding residuals. The parameter μ is an independent parameter, and the stability behaviour with respect to its variation is sought. The steady state residual is by definition zero, while $A(\boldsymbol{w}_0, \mu) = \partial \boldsymbol{R} / \partial \boldsymbol{w}$ is the system Jacobian matrix, evaluated at the steady state and conveniently partitioned into blocks expressing the dependencies of fluid and structural systems.

The fluid Jacobian matrix $\partial \boldsymbol{R}_f / \partial \boldsymbol{w}_f = A_{ff}$ describes the influence of the fluid unknowns on the fluid residuals and has by far the largest number of nonzero elements for a modal structural model. This matrix block is evaluated analytically (which is crucial for the efficiency of the scheme) as described by Woodgate and Badcock [2007]. The matrix block $\partial \boldsymbol{R}_f / \partial \boldsymbol{\eta} = A_{f\eta} + \lambda\, A_{f\dot{\eta}}$ describes the dependence of the fluid residual on the moving fluid mesh. Importantly, the fluid residual $\boldsymbol{R}_f$ must be differentiated with respect to both the generalised coordinates $\boldsymbol{\eta}$ and their corresponding velocities $\dot{\boldsymbol{\eta}} = \lambda \boldsymbol{\eta}$ as these influence both the grid displacements $\boldsymbol{x}(\boldsymbol{\eta})$ and grid velocities $\dot{\boldsymbol{x}}(\dot{\boldsymbol{\eta}})$ of the fluid mesh. The Jacobian matrix block $\partial \boldsymbol{R}_\eta / \partial \boldsymbol{w}_f = A_{\eta f}$ describes how the structure responds to changes in the flow field and is formed as $A_{\eta f} = \lambda^{-1} q \Phi^T \partial \boldsymbol{f} / \partial \boldsymbol{w}_f$. The structural Jacobian matrix $\partial \boldsymbol{R}_\eta / \partial \boldsymbol{\eta} = A_{\eta\eta}$ is conveniently split into two contributions, one from the structural stiffness and damping terms and one due to the aerodynamic force vector, and is given by $A_{\eta\eta} = -\lambda^{-1} \big\{ (\Omega + \lambda \Psi) - q \Phi^T \partial \boldsymbol{f} / \partial \boldsymbol{\eta} \big\}$. From experience the second term is usually negligible but can easily be included in the calculation.

Proceeding as for Eq. (4) leads to the following eigenvalue problem for the cou-

[a]Note that the structural equations are written as $\dot{\boldsymbol{\eta}} = -\lambda^{-1} \big\{ (\Omega + \lambda \Psi)\, \boldsymbol{\eta} - q \Phi^T \boldsymbol{f} \big\}$.

pled system

$$\begin{pmatrix} A_{ff} & A_{f\eta} + \lambda A_{f\dot{\eta}} \\ A_{\eta f} & A_{\eta\eta} \end{pmatrix} \begin{pmatrix} \hat{\boldsymbol{w}}_f \\ \hat{\boldsymbol{\eta}} \end{pmatrix} = \lambda \begin{pmatrix} \hat{\boldsymbol{w}}_f \\ \hat{\boldsymbol{\eta}} \end{pmatrix} \tag{6}$$

which can be rearranged noting that the relevant eigenvalues of interest for the stability analysis originate in the uncoupled structural system,

$$\left\{ \lambda\, I - A_{\eta\eta} + A_{\eta f}(A_{ff} - \lambda I)^{-1}(A_{f\eta} + \lambda\, A_{f\dot{\eta}}) \right\} \hat{\boldsymbol{\eta}} = 0. \tag{7}$$

The latter expression is called the Schur complement of the system matrix with respect to the matrix block $(A_{ff} - \lambda I)$. Using the definitions of the Jacobian matrix blocks from above gives

$$\left\{ \lambda^2\, I + \lambda\, \Psi + \Omega - q\big(C_2 - C_3\, (A_{ff} - \lambda I)^{-1} (A_{f\eta} + \lambda\, A_{f\dot{\eta}}) \big) \right\} \hat{\boldsymbol{\eta}} = 0 \tag{8}$$

with $C_2 = \Phi^T \partial \boldsymbol{f} / \partial \boldsymbol{\eta}$ and $C_3 = \Phi^T \partial \boldsymbol{f} / \partial \boldsymbol{w}_f$. It is clear that the aerodynamic influence matrix from Eq. (4) is modelled as

$$Q(\lambda) = C_2 - C_3\, (A_{ff} - \lambda I)^{-1} (A_{f\eta} + \lambda\, A_{f\dot{\eta}}) \tag{9}$$

demonstrating the dependence on the eigenvalue. The eigenvalue problem is then solved for varying values of an independent (i.e. bifurcation) parameter μ (typically representing the dynamic pressure) to trace the development of the aeroelastic modes.

In this paper the aeroelastic modes are traced with respect to the equivalent airspeed V_{EAS}. To allow simulations in a matched point fashion, altitude variations are imposed at fixed freestream Mach numbers where reference values of density and speed of sound are adjusted according to standard atmosphere conditions with the true airspeed V_{TAS} following from the Mach number. The equivalent airspeed is then evaluated from $V_{\mathrm{EAS}} = V_{\mathrm{TAS}} \sqrt{\varrho / \varrho_0}$ where ϱ is air density at altitude and ϱ_0 is standard sea level density.

An efficient way of finding the roots of such nonlinear algebraic systems are Newton–type methods which require the evaluation of the residual and its exact or an approximate Jacobian matrix. The evaluation of the aerodynamic influence Q, particularly the term involving the matrix inverse, is the main cost as it requires operations on the high dimensional fluid system, whereas the cost to form the terms associated with the structural Jacobian matrix $A_{\eta\eta}$ is negligible in comparison. As there are n_η relevant solutions of the eigenvalue problem, the cost of forming the aerodynamic influence term at each Newton iteration, for each value of the independent parameter μ, and for a range of system parameters becomes too high without approximations. As one approximation, a Taylor series expansion [Bekas and Saad, 2005] can be written for $\lambda = \lambda_0 + \delta\lambda$ as

$$(A_{ff} - \lambda I)^{-1} \approx (A_{ff} - \lambda_0 I)^{-1} + \delta\lambda (A_{ff} - \lambda_0 I)^{-1} (A_{ff} - \lambda_0 I)^{-1} \tag{10}$$

where $\delta\lambda$ denotes a small variation to the reference value λ_0. Pre–computation of the factors in the series expansion for the right–hand side matrix $(A_{f\eta} + \lambda\, A_{f\dot{\eta}})$, requiring $4n_\eta$ linear solves per shift λ_0, allows the application of the expansion in the vicinity of λ_0.

Two approaches have been discussed in Badcock and Woodgate [2010]. An approximate Newton method evaluates the exact residual while the series expansion is used for the Jacobian matrix. The exact residual is conveniently computed by first forming the product $\boldsymbol{b} = (A_{f\eta} + \lambda A_{f\dot{\eta}})\,\hat{\boldsymbol{\eta}}$ for the current solution of the eigenpair $(\hat{\boldsymbol{\eta}}, \lambda)$, and then solving one linear system of the form $(A_{ff} - \lambda I)\,\boldsymbol{y} = \boldsymbol{b}$, the solution of which is multiplied with the matrix C_3. The alternative series method also applies the series expansion to the residual which is possible for small $\delta\lambda$ and for problems where changes in the independent parameter μ do not influence the pre–computed values. For more details on the original Schur complement eigenvalue formulation the reader is referred to the literature.

The two methods (i.e. approximate Newton and series) just described are generally referred to as full order as they constantly involve operations on the unsimplified CFD system to form the aerodynamic influence matrix. It is clear that neither of the full order formulations is appealing when the number of system parameters (besides the bifurcation parameter) becomes high. The aerodynamic influence matrix depends on the eigenvalue, particularly the imaginary part giving the response frequency, and the steady state solution. The steady state makes it dependent on a large number of parameters in both the flow model (e.g. Mach number and angle of attack) and the structural model due to structural parameters generally influencing the mode shapes required to compute the matrix $(A_{f\eta} + \lambda A_{f\dot{\eta}})$.

In previous work [Timme *et al.*, 2011] an approximation of the aerodynamic influence term was devised which enables the stability analysis in larger parameter spaces efficiently. The variation in Q was found from interpolating numerical samples using kriging. Thus, the two main tasks of the approximation are efficient sampling of the parameter space and accurate reconstruction of the matrix elements. Also, the aerodynamic influence is evaluated for constant amplitude harmonic motion giving $Q(\omega)$ rather than $Q(\lambda)$, which is commonly done in conventional p–k type of analyses. Once the aerodynamic influence is represented by the approximation model, the eigenvalue problem can be solved as often as necessary at very low computational cost. It is remarked that the approach is not limited to the kriging technique per se.

A sample of the aerodynamic influence matrix can be formed in both the frequency and time domains. Solving the n_η linear systems of the form $(A_{ff} - i\omega I)\,Y = (A_{f\eta} + i\omega\,A_{f\dot{\eta}})$ and multiplying the $n_f \times n_\eta$ solution matrix Y by the matrix $A_{\eta f}$ to integrate the responses is referred to as the linear frequency domain approach. This is the preferred choice due to the significant computational cost involved in time domain simulations. Alternatively in the time domain, allowing the use of arbitrary CFD solvers (with modal motion functionalities), the aerodynamic influence matrix is evaluated from the generalised forces $\Phi^T \boldsymbol{f}$ following an excitation in the structural unknowns using Fourier analysis.

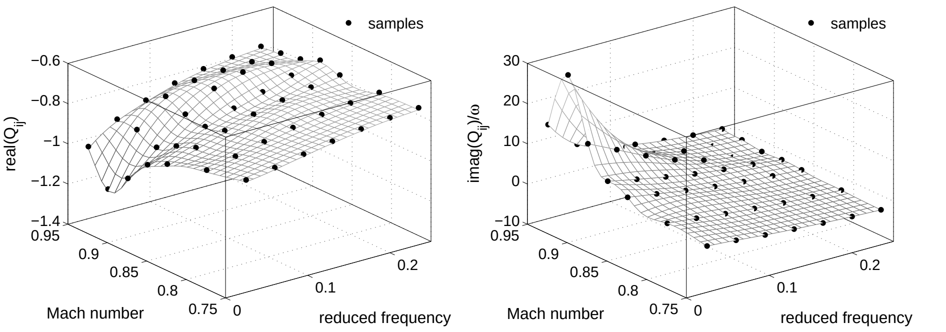

Fig. 1. Representative element $Q_{1,2}$ of aerodynamic influence matrix for baseline Goland wing/store configuration using Euler flow model.

One representative element of the aerodynamic influence matrix Q for the baseline Goland wing/store configuration, the structural model of which is defined elsewhere [Beran *et al.*, 2004], is shown in Fig. 1. The element describes the mapping between the aerodynamic response in the first modal degree–of–freedom due to changes in the second generalised coordinate. The black dots in the figure indicate sample locations while the black and white coloured, meshed surfaces represent the kriging interpolation used in the stability analysis to describe the variation of the matrix elements. The two dimensional parameter space is defined by the dimensionless response frequency and freestream Mach number. Note that the response frequency is the primary parameter dimension which always has to be included in the sampling as the eigenvalue problem is nonlinear. Solving the eigenvalue problem gives a prediction of the eigenvalue and eigenvector for any combination of the bifurcation parameter and the different system parameters, where the imaginary part of the obtained eigenvalue (i.e. the response frequency) is used itself to define the parameter space for the sampling of the interaction matrix.

4. Adapted Method of Nissim and Gilyard

As mentioned above, there are two general categories of methods to use flight flutter test data to predict the onset of aeroelastic instability. The way discussed hereafter is to identify the whole aeroelastic system by computing the equations of motion, using the method of Nissim and Gilyard [1989], rather than attempting to extrapolate to the instability point from a curve fit of a chosen stability criterion such as the modal damping and the variation with the dynamic pressure.

The eigenvalue problem for the aeroelastic stability analysis was given in Eq. (4). It is restated as

$$\left\{\lambda^2 I + \lambda \Psi + \Omega - qQ(\omega)\right\} \hat{\boldsymbol{\eta}} = 0$$

with the complex–valued aerodynamic influence matrix $Q(\omega) = Q_R + i\omega \widetilde{Q}_I$ approximated for constant amplitude harmonic motion, and $\widetilde{Q}_I = \omega^{-1} Q_I$. The subscripts R and I denote real and imaginary parts, respectively. It is remarked that, generally, the matrices Q_R and Q_I are not constant with respect to the frequency as indicated in Fig. 1. Often, the notation using the matrices $K_\eta = \Omega - q Q_R$ and $C_\eta = \Psi - q\widetilde{Q}_I$ is more familiar with structural dynamicists,

$$\left\{\lambda^2 I + \lambda C_\eta + K_\eta\right\} \hat{\boldsymbol{\eta}} = 0 \tag{11}$$

where the real and imaginary parts of the aerodynamic influence matrix are interpreted as aerodynamic stiffness and damping, respectively, and combined with the real–valued structural stiffness and damping matrices. As the aerodynamic influence, scaled through the dynamic pressure, goes to zero, the structural eigenvalue problem is restored.

4.1. *Original Method of Nissim and Gilyard*

Following the ideas presented by Gaukroger *et al.* [1980], a system identification technique, referred to as the Nissim and Gilyard method, was devised [Nissim and Gilyard, 1989]. Adapted to the notation used in the present work, the forced aeroelastic system is written as,

$$\left\{-\omega^2 I + i\omega C_\eta + K_\eta\right\} \hat{\boldsymbol{\eta}} = \Phi^T F \hat{g}(\omega) \tag{12}$$

where the right–hand side defines the forcing term. The latter equation transposed and rearranged gives the constraint equation for the system identification

$$\hat{\boldsymbol{\eta}}^T K_\eta^T + i\omega\, \hat{\boldsymbol{\eta}}^T C_\eta^T - \hat{g}(\omega) F_\eta^T = \omega^2\, \hat{\boldsymbol{\eta}}^T \tag{13}$$

where $F_\eta = \Phi^T F$ is the generalised forcing matrix. The physical forcing matrix F has dimensions $n_s \times m$ with m as a chosen number of forcing columns applied. In the original work it was recommended to apply at least two linearly independent forcing columns to negate the influence of measuring error. In the current numerical experiments, a forcing vector has entries of one according to the physical coordinates where the (single) external forcing function $g(t)$ is applied, and thus, the forcing matrix F_η is known beforehand. This information can be used to monitor the analysis results. In a flight flutter test, on the other hand, finding the modal response due to, for instance, the deflection of a control surface does not tell how the modal degrees–of–freedom were excited in the first place, and hence, this matrix is assumed to be an additional unknown.

Assuming only one forcing vector is used to simplify the following presentation, the system of constraint equations can be written for k distinct forcing frequencies, excited at a chosen fixed flight test point, as,

$$\begin{pmatrix} \hat{\boldsymbol{\eta}}_1^T & i\omega_1\, \hat{\boldsymbol{\eta}}_1^T & -\hat{g}(\omega_1) \\ \hat{\boldsymbol{\eta}}_2^T & i\omega_2\, \hat{\boldsymbol{\eta}}_2^T & -\hat{g}(\omega_2) \\ \vdots & \vdots & \vdots \\ \hat{\boldsymbol{\eta}}_k^T & i\omega_k\, \hat{\boldsymbol{\eta}}_k^T & -\hat{g}(\omega_k) \end{pmatrix} \begin{pmatrix} K_\eta^T \\ C_\eta^T \\ F_\eta^T \end{pmatrix} = \begin{pmatrix} \omega_1^2\, \hat{\boldsymbol{\eta}}_1^T \\ \omega_2^2\, \hat{\boldsymbol{\eta}}_2^T \\ \vdots \\ \omega_k^2\, \hat{\boldsymbol{\eta}}_k^T \end{pmatrix} \tag{14}$$

which is an overdetermined linear system (if $k > n_\eta$) of the general form $TX = B$ to be solved in the common least–squares sense. As the coefficient matrix T and the right–hand side matrix B are complex–valued while the solution matrix X is real–valued, it was argued instead to solve the equivalent real–valued linear system $[T_R, T_I]^T X = [B_R, B_I]^T$ to avoid the sensitivity to measuring errors.

The constraint of having a real–valued and constant solution matrix X prompted the authors of the original work to use simplified aerodynamics (i.e. quasi–steady), which can be written as $A = A_0 + i\omega A_1$, and thus, $K_\eta = \Omega - qA_0$ and $C_\eta = \Psi - qA_1$. The similarity to the matrix Q given above is intended. To identify the constant matrices of aerodynamic stiffness A_0 and damping A_1, the aeroelastic system was excited at two distinct dynamic pressures to distinguish between the structural and aerodynamic contributions in the overall stiffness and damping terms. Importantly, the generalised matrices of structural stiffness Ω and damping Ψ were assumed to be constant despite the required variation in the dynamic pressure (i.e. structural deformation during flight potentially causing changes in the modal description of the system are considered negligible).

An example is presented next for the baseline Goland wing/store configuration, the structural model of which was defined by Beran *et al.* [2004]. The wing/store configuration has four normal modes with frequencies (given in Hz) of 1.689, 3.051, 9.173 and 10.83, while structural damping is neglected. The mode shapes splined to a CFD surface grid were visualised in Timme *et al.* [2011]. To replace unavailable real flight test data, unsteady time accurate simulations were done at realistic flight conditions using the Euler equations as aerodynamic model and a computational mesh with about 24,000 control volumes. The store aerodynamics were not modelled. The excitation signal used throughout in this work is a linear chirp following the functional relation,

$$g(t) = g_a \sin\left(2\pi f_0 t + \pi\kappa t^2\right) \tag{15}$$

where g_a is the excitation amplitude and κ is the constant rate of frequency increase (chirp rate). It is evaluated as $\kappa = (f_1 - f_0)/(0.8t_1)$ with f_0 and f_1 limiting the frequency range to be excited and t_1 as the length of the time signal. To excite all relevant frequencies of the test case, the limiting excitation frequencies are chosen to be $f_0 = 0.5$ Hz and $f_1 = 15$ Hz. The amplitude of the chirp signal is set to $g_a = 5 \times 10^{-4}$ lb to maintain linearity in the simulations. One physical structural coordinate is excited per unsteady simulation. The structural points of the Goland wing selected for excitation are shown in Fig. 2. With some imagination, applying a force at these points corresponds to a control surface deflection of the real wing to excite the system.

Results are presented using three forcing columns corresponding to an excitation in the coordinates 41, 40 and 33, respectively. Following a starting period to allow the decay of transients when switching the temporal discretisation in the CFD simulations from steady state pseudo time to unsteady dual time, a time signal of $t_1 = 20$ s is simulated, applying the excitation for a period of time $0.8t_1$ and running

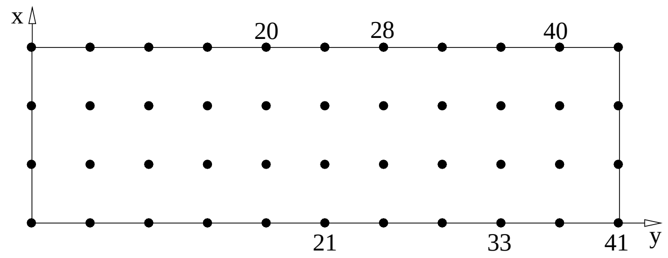

Fig. 2. Physical structural coordinates of Goland wing/store configuration.

at a sampling frequency of 1024 Hz. This relatively large sampling frequency, corresponding to a nondimensional time step of about 0.13, was found to be necessary to satisfy temporal accuracy in the unsteady simulations with acceptable discretisation errors. However, only every eighth step was taken for the Fourier analysis of the input/response signals to obtain $\hat{g}$ and $\hat{\boldsymbol{\eta}}$.

Results can be found in Figs. 3 through 5 and Tables 1 through 3 for a subsonic freestream Mach number of 0.85. Numerical simulations, using the eigenvalue analysis in a matched point fashion as described above, predict the instability to occur alongside the interaction of the first bending mode and first torsion mode with a critical velocity of $V_{\mathrm{EAS}} = 609$ ft/s (corresponding to an altitude of 22,560 ft). The system identification is done using simulated flight data at 29,000 ft and 32,000 ft to have different dynamic pressures. Representative frequency response functions $\hat{\boldsymbol{\eta}}/\hat{g}$ (showing the modulus) for the four aeroelastic modes are given in Fig. 3. Resonant behaviour close to the normal mode frequencies and two pairs of modes that interact are shown. For the results provided in the figure, the excitation was applied at the structural coordinate 40 at an altitude of 32,000 ft. To complement the results at Mach 0.85, additional responses are shown for a transonic freestream Mach number of 0.925. The baseline Goland wing/store configuration without structural damping is known to exhibit a (nearly single degree–of–freedom) torsion mode limit–cycle instability in this higher Mach number regime starting from very high altitudes [Badcock and Woodgate, 2010]. Hence, a small amount of structural damping was added (i.e. a damping ratio of 0.05 in all modal degrees–of–freedom) resulting in a critical velocity of $V_{\mathrm{EAS}} = 317$ ft/s (corresponding to an altitude of about 54,000 ft). Compared with the lower Mach number, a more distinct response around the second mode frequency can consequently be observed in the figure.

Tables 1 through 3 give the identified system matrices. The generalised forcing matrix with the three forcing columns corresponding to coordinates 41, 40 and 33 is given in Table 1. Following the definition of this matrix with $F_\eta = \Phi^T F$, it is clear that each column in this matrix corresponds to the modal deflection (one entry per mode) at the physical structural coordinate where the excitation signal is applied. The identification gives reasonable results indicating an adequate excitation

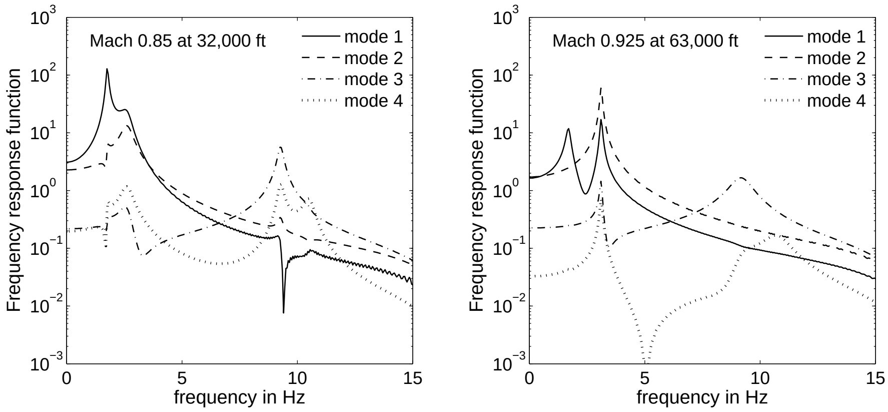

Fig. 3. Frequency response function at two freestream Mach numbers (coordinate 40).

with little numerical error. The strongest discrepancies can be found in the matrix row corresponding to the deflection in the fourth mode. The structural stiffness and damping matrices of the modal system are given in Tables 2 and 3, respectively. The reference input matrices, used to define the structure in the unsteady simulations, are simple diagonal matrices. The stiffness matrix has elements with the normal mode circular frequencies squared, while, in this case, the structural damping is zero. A reasonable identification of the diagonal entries is obtained, while relatively high errors are observed in off–diagonal matrix elements, particularly in the second column. The modal damping is not identified to be zero and an error is introduced. These inaccuracies, requiring more attention, will be discussed further following the presentation of the aerodynamic matrices.

The matrices of aerodynamic stiffness and damping are not given in the form of a table but as a representative matrix element cross–plotted with the exact numerical results of the aerodynamic influence matrix. These results, which demonstrate the shortcomings of the assumptions applied in the Nissim and Gilyard method concerning the aerodynamic influence, are presented in Fig. 4. Even at the chosen subsonic Mach number of 0.85, the approximation of the aerodynamic influence matrix using constant terms is poor. A nearly linear development with respect to the dimensionless reduced frequency $k = \frac{\omega b}{V_{\mathrm{TAS}}}$ (where b is half the reference length) can be observed. Interestingly, the reference data in the figure correspond to the samples for the response surfaces shown in Fig. 1. In there, while the constant approximation seems to be fair at a freestream Mach number of 0.85 in relation to the global variation, it certainly gets worse entering the transonic regime. In the case of the symmetric Goland wing without static deformation, the discussion of variation in dynamic pressure is irrelevant for the aerodynamic influence term as the matrix A (or equivalently Q) is indeed independent of the dynamic pressure.

The true measure of accuracy for the identification of the system are the stabil-

Table 1. Generalised forcing matrix F_η for three forcing columns.

reference matrix (ft)			matrix identified at 29,000 ft (ft)			% Error		
–0.1115	–0.0963	–0.0796	–0.1117	–0.0927	–0.0809	0.18	–3.74	1.63
0.1077	–0.1936	0.0916	0.1074	–0.1929	0.0926	–0.28	–0.36	1.09
–0.0254	0.1521	–0.0203	–0.0254	0.1501	–0.0196	0.00	–1.31	–3.45
–0.0778	–0.0195	0.0682	–0.0738	–0.0251	0.0727	–5.14	28.7	6.60

Table 2. Generalised structural stiffness matrix Ω.

reference matrix (lb-ft)				identified matrix (lb-ft)			
112.7	0.0	0.0	0.0	112.5	–10.4	–0.1	–5.2
0.0	367.6	0.0	0.0	–0.0	376.4	3.5	6.9
0.0	0.0	3321.6	0.0	0.1	0.3	3318.0	4.9
0.0	0.0	0.0	4632.6	0.4	23.9	2.2	4634.3

Table 3. Generalised structural damping matrix Ψ.

reference matrix (lb-ft-s)				identified matrix (lb-ft-s)			
0.0	0.0	0.0	0.0	–0.059	0.051	0.159	0.172
0.0	0.0	0.0	0.0	0.039	–0.150	–0.158	–0.186
0.0	0.0	0.0	0.0	–0.004	–0.017	–0.014	–0.069
0.0	0.0	0.0	0.0	0.136	–0.290	–0.387	–0.453

ity results. The mode tracing with respect to the equivalent airspeed (in a matched point analysis) using the identified system matrices at the chosen freestream Mach number of 0.85 is presented in Fig. 5. Two sets of reference results are included in the figure. The first set uses the full order eigenvalue solver applying the series method approximation as described above. In previous studies it was demonstrated that the series method gives accurate results compared with the approximate Newton method [Timme *et al.*, 2011]. The second set of results uses the kriging approximation for the aerodynamic interaction term with the samples extracted assuming constant amplitude harmonic motion. These results are included to demonstrate the accuracy of the kriging approximation with samples for $Q(\omega)$. The only notable discrepancy can be seen for the second mode frequency at higher values of equivalent airspeed due to the strongly damped character of this mode, where the assumption of constant amplitude harmonic motion for the aerodynamic influence loses accuracy. Interestingly, the results using the identified system matrices are accurate and a critical velocity of $V_{\mathrm{EAS}} = 613$ ft/s (corresponding to an altitude of about 22,300 ft) is predicted. The system identification at different pairs of subcritical altitudes resulted in similar agreement in obtaining the flutter point. In addition, the identification at the transonic freestream Mach number of 0.925 gave a critical altitude of about 55,000 ft, which is close to the reference prediction of 54,000 ft, despite the significant variation in the aerodynamic influence matrix.

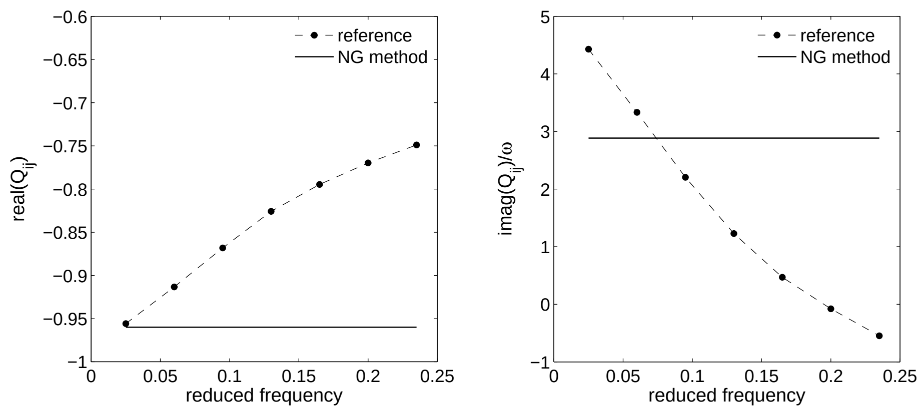

Fig. 4. Representative element $Q_{1,2}$ of aerodynamic influence matrix for baseline Goland wing/store configuration at Mach 0.85.

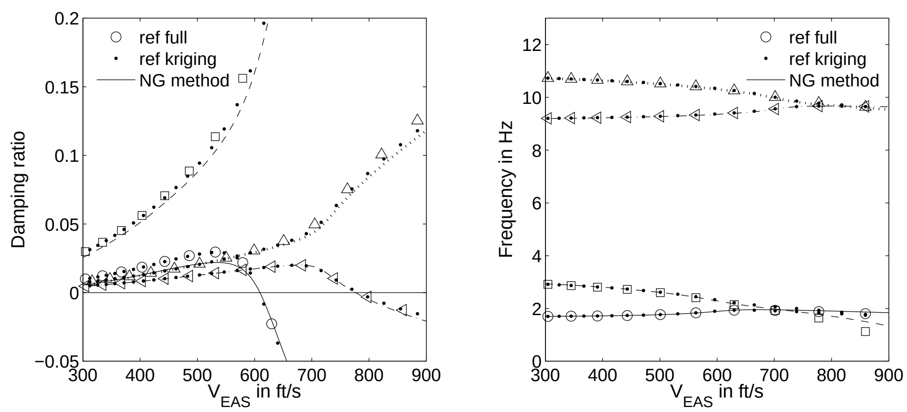

Fig. 5. Matched point mode tracing for baseline Goland wing/store configuration using Nissim and Gilyard (NG) method at Mach 0.85.

Thus, it seems that the Nissim and Gilyard method allows an acceptable identification of the system even when the aerodynamic modelling assumptions are severely violated. Returning to the errors introduced in the structural stiffness and damping matrices as found in Tables 2 and 3, respectively, it is suggested that the identification process gives the four system matrices that best describe the dominant physics. However, as a consequence of the aerodynamic modelling assumptions, a correction is added to the structural matrices to deal with these acknowledged errors. This observation is supported by noting that the structural matrices show different errors for identifications at different altitudes. In addition, the mode tracing was found to be inaccurate at higher altitudes resulting in additional incorrect bifurcation points (even though the significance of this inaccuracy is considered to be negligible). In some sense, we are not identifying the correct system matrices, but the best description of the dynamics varying with the chosen test altitudes.

4.2. *Adapted Method*

Two aspects motivated an adaptation of the original Nissim and Gilyard method. First, a framework is sought that allows the use of computational aeroelastic simulations, applying high fidelity CFD modelling for the aerodynamics, to assist in flutter clearance when updating numerical models with flight flutter test data. Secondly, the assumption of constant matrices, and thus simplified physics, to identify the system is avoided when updating a potentially nonlinear trend, provided by the numerical model, with constant corrections. This approach, different to the original Nissim and Gilyard method, requires a more or less accurate numerical model of the real system. Based on Eq. (13), write the adapted constraint equation as

$$\hat{\boldsymbol{\eta}}^T \delta K_\eta^T + i\omega\, \hat{\boldsymbol{\eta}}^T \delta C_\eta^T - \hat{g}(\omega) F_\eta^T = \hat{\boldsymbol{\eta}}^T \{\omega^2 I - i\omega\, C_\eta^T - K_\eta^T\}, \tag{16}$$

where the matrices δK_η and δC_η denote the identified constant updates for the matrices K_η and C_η of the provided model. Thus, rather than identifying the entire aeroelastic system with constant matrices, a constant correction is identified based on an assumed numerical representation of the problem. The latter equation is a simple rearrangement of the constraint equation in Eq. (13) assuming some knowledge of the real problem (i.e. a numerical model) is available. The equation simplifies to the original formulation if no numerical model is available. The latter expression can be recast following Eq. (14) to define an overdetermined system to be solved in a least–squares sense. Choosing this path, a numerical model can be adjusted using test data.

An important and computationally expensive element of the adapted method, when CFD simulations are used to evaluate the aerodynamic influence, is the matrix Q of the provided numerical model on the right–hand side of the constraint equation. It would become prohibitive to directly evaluate this matrix for each frequency and combination of other system parameters (such as freestream Mach number). Instead, the kriging interpolation approximation, as described above, is applied to provide the variation in the elements of the aerodynamic influence matrix at any parameter location based on few expensive numerical samples. These samples are precomputed using the provided numerical model of the aeroelastic system.

5. Application of Adapted Method

The unsteady simulation results, created and analysed for the original Nissim and Gilyard method as described previously, are now used for the adapted method taking the same set of three forcing columns. To test the adapted method, the structural stiffness and damping matrices from the provided numerical model (i.e. the matrices

Table 4. Generalised forcing matrix F_η.

matrix identified at 29,000 ft (ft)			% Error		
–0.1109	–0.0958	–0.0793	–0.54	–0.52	–0.38
0.1071	–0.1926	0.0911	–0.56	–0.52	–0.55
–0.0253	0.1510	–0.0202	–0.39	–0.72	–0.49
–0.0772	–0.0194	0.0677	–0.77	–0.51	–0.73

Table 5. Generalised matrices of structural stiffness Ω and damping Ψ.

identified stiffness matrix (lb-ft)				identified damping matrix (lb-ft-s)			
112.7	–0.3	–0.3	–0.7	–0.001	0.051	0.011	–0.024
–0.0	366.3	–0.4	1.1	0.000	–0.016	0.009	–0.000
–0.0	–0.2	3314.7	0.5	–0.000	0.019	0.008	–0.034
0.1	0.0	–1.1	4619.9	–0.004	–0.063	0.009	0.035

found on the right–hand side of the constraint equation) were based on arbitrarily chosen normal mode frequencies and damping ratios. Here, the nominal normal mode frequencies of the Goland wing/store case were rounded to one significant digit (e.g. for the first mode we take 2 Hz), while for the modal damping ratios different values between 0.1 and 0.5 were used for the four degrees–of–freedom. In addition, the elements of the aerodynamic influence matrix of the provided numerical model were modified by a constant value randomly chosen.

The structural matrices are given in Tables 4 and 5 based on the identification at Mach 0.85. The generalised forcing matrix is found to be better identified compared with the results given in Table 1. While the first three matrix rows corresponding to the deformations in modes 1 to 3 were already identified accurately with the original method, clear improvements in the last row are observed. The errors in the matrix entries are consistently reduced below 1%. The generalised matrices of stiffness and damping are nicely identified as shown in Table 5 where the identified corrections added to the provided matrix values are presented. The peak errors in the stiffness matrix, particularly in the second column, are reduced, while the entries of the damping are reduced consistently by almost an order of magnitude throughout.

A representative element of the aerodynamic influence matrix is given in Fig. 6 comparing reference data using the full order samples and the identified results using the Nissim and Gilyard method in its original and adapted form. As for the identified structural matrices, results are shown for the aerodynamics of the provided numerical model plus the correction. The adapted Nissim and Gilyard method predicts the correction δQ to be very close to the imposed constant error (with opposite sign). This is expected as the correct aerodynamics of the system, modified by a random constant value, were applied on the right–hand side of Eq. (16) for the identification. The same accuracy in the system identification for both the structural and aerodynamic correction matrices was observed for the transonic freestream Mach

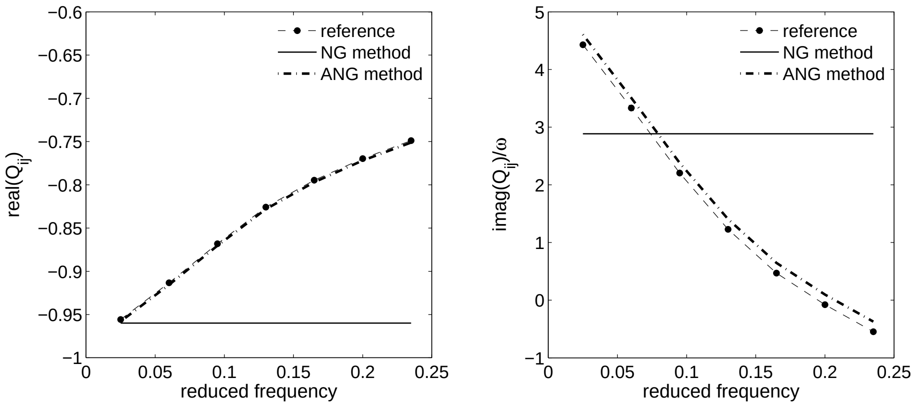

Fig. 6. Representative element $Q_{1,2}$ of aerodynamic influence matrix for baseline Goland wing/store configuration using adapted Nissim and Gilyard (ANG) method at Mach 0.85.

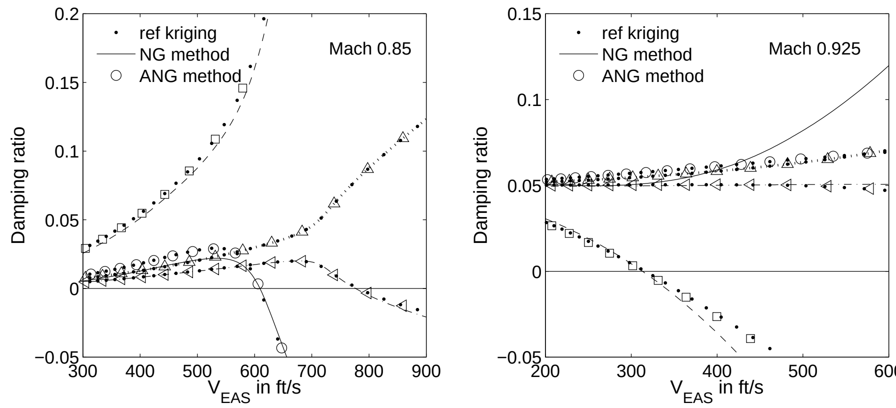

Fig. 7. Matched point mode tracing for baseline Goland wing/store configuration using adapted Nissim and Gilyard (ANG) method at Mach 0.85 and 0.925.

number of 0.925 identifying the system using simulated flight test data at 60,000 ft and 63,000 ft, the results of which are not shown herein.

As a remark of caution, for the results presented herein, the system is well defined (e.g. the imposed error in the aerodynamic matrix is indeed constant), which demands an accurate identification of the system for the method to be useful. Once the error between the numerically predicted aerodynamics and the experimental data becomes non–constant due to modelling discrepancy, a similar behaviour as for the original Nissim and Gilyard method should be expected. An incorrect assumption of a constant update for the aerodynamics would introduce an additional correction in the structural matrices. However, as we are identifying an update to a numerical aeroelastic model, confidence about the general accuracy in the modelling is increased.

The tracing of the four relevant modes with respect to the equivalent airspeed is presented in Fig. 7 for freestream Mach numbers of 0.85 and 0.925. The results using the identified correction matrices are indistinguishable from the reference kriging results following the close agreement in the system matrices. Using the identified system from the original Nissim and Gilyard method, on the other hand, the damping ratio of the first mode (with the damping ratio defined according to classical text books such as Bisplinghoff and Ashley [1962]) is predicted too low for airspeed values below the critical point. For the transonic freestream Mach number of 0.925 (showing the instability occuring in the second mode), inaccurate mode tracing at airspeeds higher than the instability onset is observed as well. These observations support the previously stated point concerning the best identification of the dominant dynamics at a chosen altitude but not of the actual system matrices. As said before, the critical point (equivalent airspeed or altitude) is nevertheless reasonably predicted.

A second test case is the MDO wing as a model of a commercial transport wing. A transonic freestream Mach number 0.85 is chosen for the analysis. Static aeroelastic deformation is considered which, in contrast to the Goland wing/store configuration, gives a dependence of the aerodynamic influence matrix on the dynamic pressure. The modal structural model retains eight normal modes. The normal mode frequencies (all given in Hz) are 0.844, 2.162, 3.559, 3.989, 5.008, 5.369, 6.573 and 7.300. No structural damping is included. The mode shapes splined to the CFD surface mesh have been visualised in Timme *et al.* [2011]. A computational mesh with 65,000 control volumes is used for the current Euler simulations. The excited frequency range is between $f_0 = 0.1$ Hz and $f_1 = 10$ Hz simulating $t_1 = 20$ s of physical time with a sampling frequency of 1024 Hz chosen for temporal accuracy in the CFD simulations. Every eighth time step was retained for the system identification. As for the Goland wing/store configuration, three forcing columns are used for the identification while individually exciting structural coordinates of the finite element model to simulate control surface deflection at realistic flight conditions as the means of system excitation. The excitation is done about the statically deformed wing following the simulation of a steady state.

As above, to challenge the adapted method, the normal mode frequencies of the provided numerical model were rounded to one significant digit, while random values for the modal damping ratios between 0.05 and 0.5 were imposed. The identified matrices of generalised forcing and structural stiffness for this second configuration are shown in Tables 6 and 7. The identification of the forcing matrix is accurate with a worst error of 1.52%. The same accuracy can be found in the structural stiffness matrix identified using response signals at altitudes of 5,000 m and 6,000 m. Diagonal entries are close to the nominal values (to be evaluated as the square of the normal mode circular frequency), while off–diagonal elements are very small

Table 6. Generalised forcing matrix F_η for three forcing columns.

reference matrix ($\times 10^{-3}$ m)			matrix identified at 6,000 m ($\times 10^{-3}$ m)			% Error		
4.786	9.144	10.990	4.785	9.138	10.985	–0.02	–0.07	–0.05
–1.985	6.322	11.900	–1.985	6.320	11.886	–0.00	–0.03	–0.12
4.399	–3.193	–10.990	4.398	–3.189	–10.985	–0.02	–0.13	–0.05
0.526	–4.348	3.852	0.534	–4.336	3.856	1.52	–0.28	0.10
1.354	–2.151	–1.439	1.354	–2.148	–1.439	0.00	–0.14	0.00
0.640	0.262	–5.156	0.634	0.259	–5.153	–0.94	–1.15	–0.06
–3.233	10.230	–3.433	–3.227	10.211	–3.420	–0.19	–0.19	–0.38
–4.276	1.844	1.884	–4.270	1.842	1.879	–0.14	–0.11	–0.27

Table 7. Generalised structural stiffness matrix Ω.

identified stiffness matrix (N-m)							
28.6	0.3	0.4	–5.2	–1.0	–0.4	2.4	0.1
–0.3	184.2	0.4	0.7	0.2	0.4	–0.0	0.0
–0.0	0.3	498.9	0.7	0.1	0.1	–0.9	–0.0
–0.2	0.1	–0.5	627.4	0.1	–0.2	0.5	–0.7
–0.1	0.2	0.1	0.2	988.7	0.1	–0.3	0.2
0.0	0.4	0.2	0.8	0.3	1136.1	–1.2	0.5
0.4	–0.1	–1.2	–0.2	–0.3	–0.8	1702.4	–0.6
0.1	0.1	–0.0	0.5	0.1	–0.1	–0.5	2099.3

in comparison. Also, the results are improved compared with the original method. The diagonal entry in the first mode, for instance, was identified to a value of 33.5 corresponding to an error of 19.2%, while most of the off–diagonal elements were reduced by almost an order of magnitude using the adapted method. Similar to the stiffness matrix, the identification of the structural damping matrix (not shown herein) was improved significantly throughout.

The aerodynamics of the provided numerical model were modified as well in order to discuss how the model updating based on system identification could be exploited to establish trends when required to extrapolate to the instability point. A design altitude of the configuration was (rather arbitrarily) chosen to be 13,000 m, while the provided numerical model is assumed to predict the physics at this design point accurately. An error in the elements of the aerodynamic influence matrix, linearly varying with altitude, was imposed. This modification and its identification are illustrated for a representative matrix element in Fig. 8 showing the dependence on altitude at a fixed reduced frequency. The development of the modified matrix element of the provided numerical model can be seen. The model updates are identified at four subcritical altitudes reproducing the expected linear trend of the imposed error. This trend is then linearly extrapolated with respect to altitude to correct the provided numerical model.

The results of the stability analysis showing the tracing of the four aeroelastic modes with the lowest nominal frequencies are presented in Fig. 8. The reference

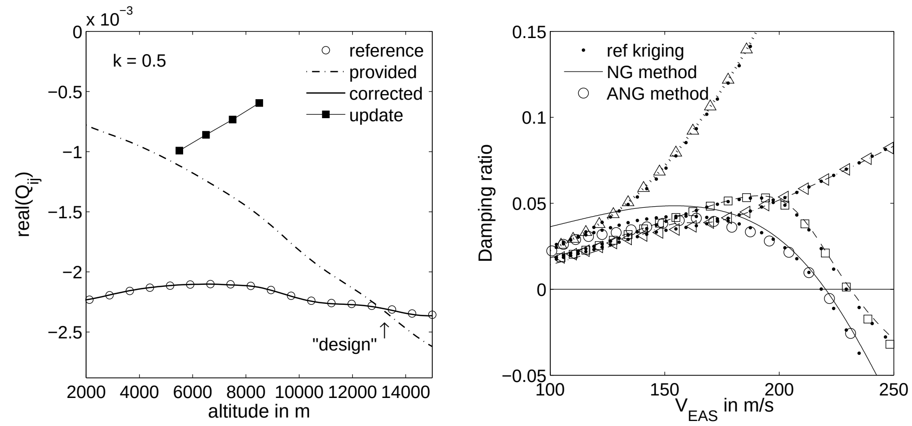

Fig. 8. Adapted Nissim and Gilyard (ANG) method applied to MDO wing configuration.

analysis, using the kriging approximation for the aerodynamic influence matrix in a frequency/altitude parameter space, predicts the instability in the first mode at a critical velocity of $V_{\mathrm{EAS}} = 218$ m/s (corresponding to about 4,500 m in altitude). The analysis, using the identified system from the original Nissim and Gilyard method, overpredicts the critical conditions slightly to about $V_{\mathrm{EAS}} = 222$ m/s with the system matrices identified at altitudes of 5,000 m and 6,000 m. This prediction deteriorates when using altitudes at increasing distance to the instability. It can also be seen that the damping ratio in the critical mode is only reproduced well in close range to the identification point. Using the system matrices obtained from the adapted method, on the other hand, results in an accurate prediction compared with the reference solution. Compared with the four aeroelastic modes in the previous Goland wing/store configuration, the increased number of normal modes, while applying the same number of independent forcing columns, does not corrupt the method. However, the behaviour for a more realistic number of retained normal modes (typically about 100) remains to be seen.

As for the previous configuration, we are looking at a well defined numerical problem imposing constant or linearly varying errors, and accuracy in the current discussion is hence required. The general idea of the approach, however, should become clear. A numerical model of a configuration should be available while lacking accuracy, compared with the real system, due to modelling discrepancies. The numerical model is then tuned to match observations based on subcritical flight tests. Extrapolation to predict the critical point, as is generally required for flutter prediction techniques based on flight test data, still becomes an issue. This was demonstrated for the MDO wing configuration undergoing static aeroelastic deformation. However, the task of extrapolation would use a trend established from tuning the model in subcritical conditions building confidence in the numerical model.

6. Conclusions

The work presented in this paper describes an approach based on the Nissim and Gilyard method to update computational aeroelastic predictions with flight test data by identifying corrections for the matrices of the underlying numerical model. The central idea is to use the predictive capabilities of computational aeroelastic tools, capturing the dominant physics of the problem at hand, while adding information from flight tests of the real aircraft to correct for missing physics and systematic errors in the numerical model. Computational fluid dynamics is used to evaluate the aerodynamic influence matrix of the provided numerical model, while kriging interpolation is applied to account for parameter variations. As real flight test data are not available for the test cases discussed, unsteady simulations using the Euler flow model are exploited instead. The results using the identified system, presented for the Goland wing/store configuration and the multidisciplinary optimisation wing, are generally improved compared with the original Nissim and Gilyard method, and good agreement with reference predictions is found.

In the general case, extrapolation of non–constant system matrices is required to predict the flutter onset. This extrapolation is equivalent to other flutter prediction methods, such as the damping curve fit, and becomes critical when a sudden loss of damping is encountered (where also sudden changes in the aerodynamic influence matrix are not unlikely). The presented approach could be exploited to evaluate a correlation between the numerical model and real data within the stable flight regime to account for the shortcomings in the modelling, the information of which could then be used with increased confidence in the numerical model to extrapolate to the flutter onset.

Acknowledgements

The first author wishes to thank Professor J. E. Cooper for discussing the ideas and explaining some technicalities of flight flutter testing. This research formed part of the programme of the Marie Curie Excellence Team ECERTA financially supported by the European Union under contract MEXT–CT–2006–042383.

References

Badcock, K. J., Richards, B. E. and Woodgate, M. A. [2000] "Elements of computational fluid dynamics on block structured grids using implicit solvers," *Progress in Aerospace Sciences* **36**(5–6), 351–392.

Badcock, K. J. and Woodgate, M. A. [2010] "Bifurcation prediction of large–order aeroelastic models," *AIAA Journal* **48**(6), 1037–1046.

Bekas, C. and Saad, Y. [2005] "Computation of smallest eigenvalues using spectral Schur complements," *SIAM J. Sci. Comput.* **27**(2), 458–481.

Bendiksen, O. O. [2008] "Transonic limit cycle flutter of high–aspect–ratio swept wings," *Journal of Aircraft* **45**(5), 1522–1533.

Beran, P. S., Khot, N. S., Eastep, F. E., Snyder, R. D. and Zweber, J. V. [2004] "Numerical analysis of store–induced limit–cycle oscillation," *Journal of Aircraft* **41**(6), 1315–1326.

Bisplinghoff, R. L. and Ashley, H. [1962] *Principles of Aeroelasticity* (John Wiley & Sons, Inc., New York, NY), p. 236.

Dimitriadis, G. and Cooper, J. E. [2001] "Flutter prediction from flight flutter test data," *Journal of Aircraft* **38**(2), 355–367.

Gaukroger, D. R., Skingle, C. W. and Heron, K. H. [1980] "An application of system identification to flutter testing," *Journal of Sound and Vibration* **72**(2), 141–150.

Goura, G. S. L. [2001] "Time marching analysis of flutter using computational fluid dynamics," Ph.D. thesis, Department of Aerospace Engineering, University of Glasgow, Glasgow, United Kingdom.

Jameson, A. [1991] "Time dependent calculations using multigrid with applications to unsteady flows past airfoils and wings," AIAA Paper 91–1596.

Kayran, A. [2007] "Flight flutter testing and aeroelastic stability of aircraft," *Aircraft Engineering and Aerospace Technology: An International Journal* **79**(2), 150–162.

Kehoe, M. W. [1995] "A historical overview of flight flutter testing," Tech. Rep. NASA–TM–4720, Dryden Flight Research Center, Edwards, CA.

Nissim, E. and Gilyard, G. B. [1989] "Method for experimental determination of flutter speed by parameter identification," Tech. Rep. NASA–TP–2923, NASA Ames Research Center, Edwards, CA.

Osher, S. and Chakravarthy, S. R. [1983] "Upwind schemes and boundary conditions with applications to euler equations in general geometries," *Journal of Computational Physics* **50**(3), 447–481.

Palacios, R., Climent, H., Karlsson, A. and Winzell, B. [2003] "Assessment of strategies for correcting linear unsteady aerodynamics using CFD or experimental results," in *Progress in Computational Flow–Structure Interaction*, eds. W. Haase, V. Selmin, and B. Winzell (Springer–Verlag, New York, NY), pp. 209–224.

Timme, S. and Badcock, K. J. [2011] "Transonic aeroelastic instability searches using sampling and aerodynamic model hierarchy," *AIAA Journal* **49**(6), 1191–1201.

Timme, S., Marques, S. and Badcock, K. J. [2011] "Transonic aeroelastic stability analysis using a kriging–based Schur complement formulation," *AIAA Journal* **49**(6), 1202–1213.

van Leer, B. [1979] "Towards the ultimative conservative difference scheme. V: a second–order sequel to Godunov's method," *Journal of Computational Physics*, **32**(1), 101–136.

von Schlippe, B. [1936] "Zur Frage der selbsterregten Flügelschwingungen," *Luftfahrtforschung* **13**(2). Translated and Reprinted in NACA–TM–806.

Woodgate, M. A. and Badcock, K. J. [2007] "Fast prediction of transonic aeroelastic stability and limit cycles," *AIAA Journal* **45**(6), 1370–1381.